https://africanjournalofbiomedicalresearch.com/index.php/AJBR
Afr. J. Biomed. Res. Vol. 27(November 2024); 1230-1247

Research Article

Immunopathological effect of whole sonicated *Staphylococcus Lugdunensis* Antigen uploaded with Zinc oxide nanoparticle in male albino Rats

Namir I. Mohammed[1*], Ahmed Q. Al-Awadi[1]

[1]*Department of pathology and poultry disease College of Veterinary Medicine / University of Baghdad, Baghdad, Iraq*

ABSTRACT

To investigate the effects of Zinc Oxide nanoparticles as adjuvants for inducing immunological responses against *Staphylococcus Lugdunensis*, **fitty** A number of healthy white male rats, aged approximately 8-10 weeks, were randomly divided into five groups and subjected to the following treatments. The control negative group, Group 1 (n=10), was infected with 0.3 ml of aseptic normal saline**.** Group 2 (n=10): infection of rats with *Staphylococcus lugdunensis,* intra peritoneal (I/P) Challenge Dose of *Staphylococcus. Lugdunensis* ($1.5x10^8$ Cell/ml) was used according (**McFarland standards**). (control positive group). Group 3 (n=10): was immunized S/C with (0.3ml) of whole sonicated Staphylococcus lugdunensis antigens (3mg/ml) 2dose with 2 weeks interval then infected with Staphylococcus lugdunensis. Group 4 (n=10): was immunized S/C with (0.3ml) of whole sonicated *Staphylococcus lugdunensis* antigens(3mg/ml) that uploaded on ZnO nanoparticles then 2dose with 2 weeks interval infected with *Staphylococcus lugdunensis.* Group 5 (n=10): were Injection with (0.3ml) of S/C ZnO-NPs. At 28-day post immunization, and serum was collected for detection of TNF-α, levels. After 30-day post immunization the rats were infected with *Staphylococcus lugdunensis* Intra peritoneal(I/P) ($1.5x10^8$ Cell/ml). Five rats were sacrificed from each group at day 7, and 21 post infection and samples from internal organs (liver and spleen) were taken for histopathology. That show high levels of TNF-α in the 2 nd and 3rd group compared to 1st and 4th groups. the result express focal granulomatous in the liver parenchyma, Hepatocyte Fatty change, necrosis of the hepatocytes, Thrombus in the portal area, in animal at the1st Although animals in the second and third groups showed mild to absent granulomatous lesions, it was determined that vaccinated animals with sonicated Ags containing ZnO-NPs achieve a strong immune response that fully protects against Staphylococcus lugdunensis infection. This is the first step towards developing a vaccination therapy.

KEYWORDS**:** *Staphylococcus. Lugdunensis, Sonicated-Ag,* ZnO-NPs, green synthesis, immune response

Author for correspondence: E mail: namer.i@uokerbala.edu.iq, Orcid ID: 0000-0003-0732-6700

Received: 04/11/2024 Accepted: 11/11/2024

DOI: https://doi.org/10.53555/AJBR.v27i3.3628

Introduction:

Staphylococcus. Lugdunensis is classified as a coagulase-negative staphylococcus (CoNS species). The organism is part of the indigenous human skin microbiota, inhabiting several specific regions including the perineal and inguinal areas. **(Bieber and Kahlmeter, 2010),** However, it is today acknowledged as a powerful human pathogen. In many aspects, the behavior of *Staphylococcus lugdunensis* displays similar characteristics to Staphylococcus aureus. , displaying more virulence than other clonal non-specific bacteria (CoNS). **(Frank *et al.*, 2008).** *S. lugdunensis* is capable of inducing a wide range of infections, spanning from localized to systemic disorders. It also has the ability to produce biofilms, which in turn leads to a variety of infections associated with foreign bodies, such as catheter-related bacteremia, bone infections, and joint infections. **(Argemi *et al.*, 2017)** and severe infective endocarditis **(Non and Santos, 2017).** Primarily, it has been documented in cases of skin and soft tissue infections.

(Papapetropoulos *et al.*, 2013). Previous in vitro investigations have indicated the presence of many virulence factors, such as hemolysis and adhesion proteins, namely Fg-binding protein (Fbl). **(Mitchell *et al.*, 2004b)**, von Willebrand factor-binding protein vWbl **(Nilsson *et al.*, 2004a)** and iron-regulated surface determinant proteins **(Heilbronner *et al*., 2016)**. Consequently, *S. lugdunensis* has been commonly described as a wolf disguised as a sheep. **(Frank *et al.*, 2008).**

The colonization of the skin by *S. lugdunensis*, particularly in the groin, toes, and axillae, has been shown to be three times more prevalent among healthy persons compared to S. aureus, which mostly colonizes the nose. (**Bieber and Kahlmeter,2010**).

The overall pathogenicity of *S. lugdunensis* has not been well studied in the field of veterinary medicine. The results of a comparative study on *S. lugdunensis* infections in small companion animals revealed that *S. lugdunensis* is predominantly present in deep tissues and wounds, rather than surface infections. Therefore, it should be considered a credible pathogen. (**Rook *et al.*, 2012)**. Furthermore, *S. lugdunensis* has been demonstrated to induce subcutaneous abscesses, peritonitis, and osteomyelitis in mice. **(Rozalska and Ljungh, 1995)** and rabbits (**Gahukamble *et al.*, 2014)** Despite being detected in a blood sample of a dog with endocarditis, the role of *S. lugdunensis* in the pathogenesis of the disease remains uncertain. The underestimation of the incidence of *S. lugdunensis* in both human and veterinary medicine is attributed to its vulnerability to comparable colony form, hemolytic activity, and ability to agglutinate latex particles covered with fibrinogen, which can result in misidentification as *S. aureus.* **(Zbinden *et al.*, 1997).** In addition to being economical, safe, and easily synthesisable, zinc oxide nanoparticles are the second most prevalent metal oxide after iron. **(Kalpana and Devi Rajeswari, 2018).** Zinc oxide (ZnO) is well recognized for its wide range of applications in both industrial and daily chemical sector as a chemical additive generated from zinc. Nevertheless, the advancement of nanotechnology has led to the increasing adoption of ZnO-NPs as a viable alternative to ZnO materials in several fields such as industrial manufacturing, environmental management, therapeutic care, food production, and biomedicine are all areas of focus. **(Siddiqi *et al*., 2018)**, they are prepared from ZnO by a variety of methods, such as physical **(Aadim and Abbas, 2023),** Chemical methods (**Khitam *et al*.,2018; Al-Hraishawi *et al.*, 2023)** and biological template techniques. The green synthesis approach enables the large-scale manufacture of ZnO nanoparticles without any additional undesirable substances. **(Husain *et al.*, 2019; Yusof *et al*., 2019; Alwash, 2020; Al-Ghareebawi *et al*., 2021; Majeed *et al.*, 2022).**

Material and methods

Bacteria were obtaining from Department of Biology, College of Science, University of Baghdad, Iraq, it was diagnosed by Vitec and was activated before the experiment began, then confirmation by polymerase chain reaction (PCR) Assay.

Preparation of *Staphylococcus. Lugdunensis* Antigens:

It was prepared as follow **(Mitov *et al.*, 1992):**

Staphylococcus Lugdunensis cultured on nutrient agar, incubated at 37 °C for 24 hrs. and harvested by PBS(PH7.2), centrifuged at 3000 rpm 4 °C /30 minutes then washed the precipitate three times with PBS, and the precipitate was re-suspended with PBS and put in the universal tube, the universal tube that contained *S. Lugdunensis* suspension was placed in the ultrasonicator device (at 12 Peak for 2 minutes' intervals between them, for 30 minutes in cold environment (ice), the sonicated suspension was centrifuged at 10000 rpm for 30 minutes in cold- centrifuge, and then the supernatant was filtered by Millipore filter and examined by Gram stain and culturing on blood agar to confirm sterility of this antigen. The Biuret technique was employed to quantify the overall protein concentration of this antigen, known as sonicated Ags, and it was determined to be 3 mg/ml.

preparation of Zinc Nano particle

Zinc oxide nanoparticle was prepared in Department of Biotechnology, College of Science, University of Baghdad. Synthesis of zinc oxide nanoparticle by biological methods.

The fresh leaf *Allium porrum* were purchased from vegetable market in Kerbala, Iraq The fresh green leaves were clean, cutting and air-dried in shadow and made into fine powder. then 250 g of fresh leaf *Allium porrum* was Mixtured with 500 ml of deionized water and The combination was a stirrer one hour then put in 4°C for 24 hrs. After that centrifugation at 8000 rpm for 10 min. The supernatant was take and put in shadow container in Refrigerator. 200ml of supernatant was added to 20g from zinc acetate and put the mixture on the shaker device overnight. Divide the filtrate on the tubes and place it in the centrifuge. After discarding the supernatant, the precipitate was washed by adding 5 mL of deionized water by centrifugation at 8000 revolutions per minute for 5 minutes. Discard the supernatant while collecting the sediment, which was then placed in a clean petri dish and kept at 37 °C for 24 hours to facilitate drying. last step dry grinding by the pod very well .in this time nanoparticles be ready for characterization. Amounts of ZnO-NPs (size of Nanoparticle was 65.49 nm), 0.312mg ZnO-NPs was added to 5ml of suspension Ag. The resulting mixtures was gently stirred at 37°C on a sonicated water path device.

Characterization of zinc oxide nanoparticle

- Atomic Force Microscope(AFM)
- Fourier Transform Infrared Spectroscopy (FTIR)
- Field emission Scanning Electron Microscopy (FE-SEM) Analysis
- X-Ray Diffraction

Ethics approval

The Animal Care and Use Committee (College of Veterinary Medicine) University of Baghdad reviewed and approved the study. (P.G.2349/ date 24.12.2023)

Experimental Design:

fifty healthy white male rats, age ranged between 8-10 weeks, were randomly divided into five groups and treated as the following.

- Group 1 (n=10): was inoculated with (0.3 ml) of sterile normal saline and served as control negative group.
- Group 2 (n=10): infection of rats with *Staphylococcus lugdunensis,* intra peritoneal (I/P) Challenge Dose of *Staphylococcus. Lugdunensis* ($1.5x10^8$ Cell/ml) was used according (**McFarland standards**). (control positive group).
- Group 3 (n=10): was immunized S/C with (0.3ml) of whole sonicated *Staphylococcus lugdunensis* antigens (3mg/ml) 2dose with 2 weeks interval then infected with *Staphylococcus lugdunensis.*
- Group 4 (n=10): was immunized S/C with (0.3ml) of whole sonicated *Staphylococcus lugdunensis* antigens(3mg/ml) that uploaded on ZnO nanoparticles then 2dose with 2 weeks interval infected with *Staphylococcus lugdunensis.*
- Group 5 (n=10): was inoculated with (0.3ml) of S/C ZnO-NPs.

At 28-day post immunization, and serum was collected for detection of TNF-α, levels. sunlong medical company Cat: NSL1184r

After 30-day post immunization the rats were infected with *Staphylococcus lugdunensis* Intra peritoneal(I/P) ($1.5x10^8$ Cell/ml) was used according (**McFarland standards**). Five rats were sacrificed from each group at day 7, and 21 post infection and samples from internal organs (liver and spleen) were taken for histopathology.

Results

AFM Analysis Interpretation

The Atomic Force Microscopy (AFM) analysis of the synthesized nanoparticles of zinc oxide (ZnO-NPs) offers comprehensive insights into their surface morphology and dimensions. The AFM data reveals an average height of the nanoparticles to be 28.934 nm. The height distribution shows that 10% of the particles have a height of 20.0 nm or less, 50% have a height of 27.5 nm or less, and 90% have a height of 40.0 nm or less. These Analysis reveals a very limited range of sizes, which is beneficial for guaranteeing uniform performance of nanoparticles in various applications. Moreover, the distribution of granularity accumulation offers additional evidence to corroborate the systematic morphological investigation. With a mean diameter of 65.49 nm, the ZnO-NPs are distributed as follows: 10% have a diameter of 20.0 nm or less, 50% have a diameter of 45.0 nm or smaller, and 90% have a diameter of 130.0 nm or smaller. The surface area of the ZnO nanoparticles, computed using the BET (Brunauer-Emmett-Teller) technique, ranges from 30 to 60 m^2/g, contingent upon the particular distribution and density of particle sizes. In applications that need rapid reactivity and surface interactions, such as catalysis and adsorption, the substantial surface area of this material is beneficial. **Malekshah *et al.*,2021**).

The comprehensive atomic force microscopy (AFM) experiments validate the effective synthesis of ZnO nanoparticles with a uniform and controlled range of sizes, meeting the stringent requirements expected in global scientific research. Their complex surface structure and large surface area make these nanoparticles very suitable for a diverse array of advanced applications in the domains of nanotechnology and materials research. **Hernández-Aguirre *et al.*,2016)**

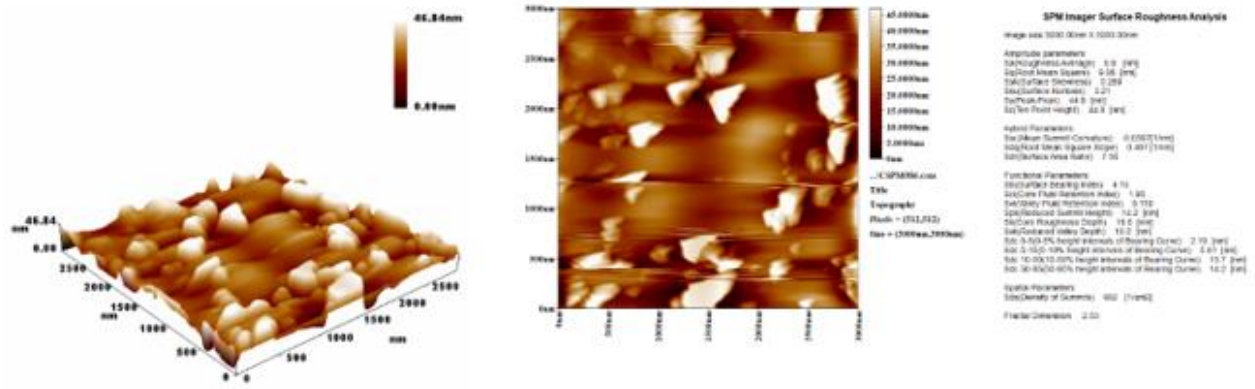

Figure 1) Atomic force microscopy (AFM) of Zinc Oxide nanoparticles made from fresh Allium porrum leaves shows the structure in both two and three dimensions. On average, the nanoparticles are 65.49 nm across.

.

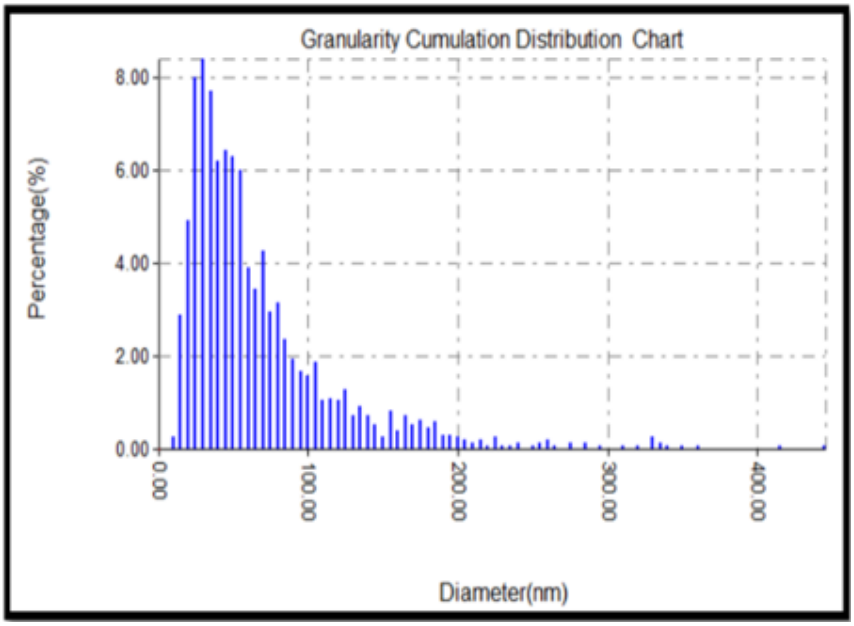

Figure 2) Particle Size Distribution of ZnO Nanoparticles Prepared Using Extract

FE-SEM and EDX Analysis

Evaluating the synthesized zinc oxide nanoparticles (ZnO-NPs) with Field Emission Scanning Electron Microscopy (FE-SEM) yields accurate data on their structure and size. When subjected to an accelerating voltage of 20.0 kV and a beam current of 10.000 nA, the FE-SEM images captured at a 1000x magnification show that the ZnO-NPs exhibit a uniform and spherical morphology. The mean diameter of the aerosol particles is 65.49 nanometers. The high-resolution images demonstrate that the nanoparticles are uniformly dispersed and possess a planar surface pattern. Furthermore, it is crucial to ascertain the precise surface area of the ZnO nanoparticles by the utilization of the BET (Brunauer-Emmett-Teller) technique to assess their surface properties. From the average particle size measured, the surface area is expected to vary between 30 and 60 m^2/g, depending on the specific distribution and density of the particles. The substantial surface area of this material is advantageous for applications requiring high reactivity and efficient surface interactions, such as catalysis and adsorption. The ZnO nanoparticles exact morphological characteristics, consistent nanoscale dimensions, and extensive surface area validate the efficacy of the synthesis technique used to produce them, in compliance with international research standards. The thorough characterization of ZnO-NPs guarantees their suitability for a wide range of applications in nanotechnology and materials science, satisfying the strict quality standards required in scientific research. **Patel and Patel, 2021.**

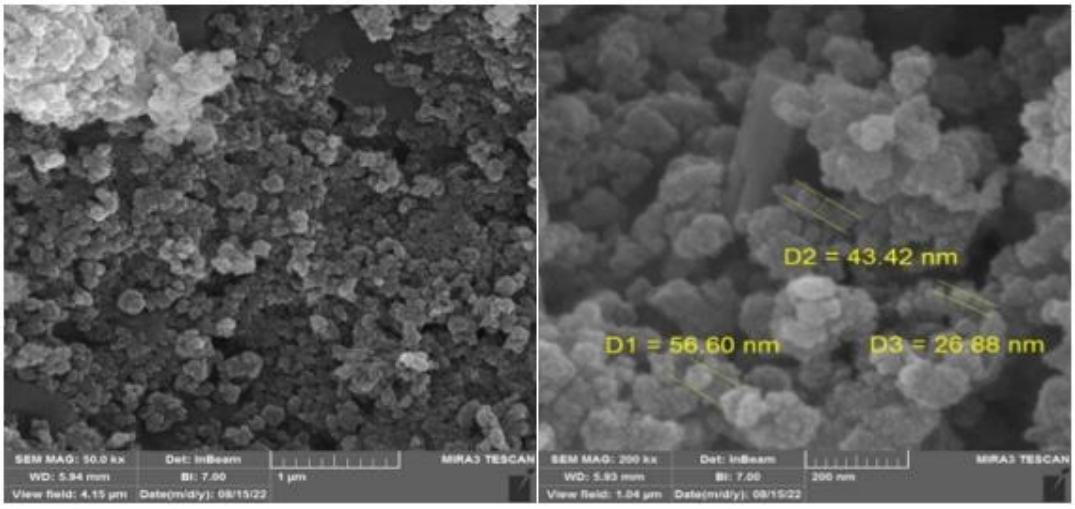

Figure 3) High-Resolution FE-SEM Imaging of ZnO Nanoparticles (sized less than 100nm)

Quantitative elemental analysis revealed the weight percentages (Wt%) and atomic percentages (At%) of the detected elements. Carbon (C) was present at 13.89 Wt% (24.09 At%), nitrogen (N) at 3.61 Wt% (5.37 At%), oxygen (O) at 28.90 Wt% (37.64 At%), sodium (Na) at 26.94 Wt% (24.41 At%), and zinc (Zn) at 26.66 Wt% (8.50 At%). The analysis employed the PAP

correction method and was conducted in a standardless manner, resulting in a chi-square (χ^2) value of 45.12. Automatic identification results indicated the presence of multiple elements with their corresponding line intensities and probabilities. Key elements identified included neon (Ne), sodium (Na), phosphorus (P), zirconium (Zr), nitrogen (N), oxygen (O), tantalum (Ta), zinc (Zn), copper (Cu), terbium (Tb), and rhenium (Re).The measurements provide detailed data on the elemental composition and analytical characteristics of the ZnO nanoparticles produced during synthesis. **Zabihi *et al.*,2019).**

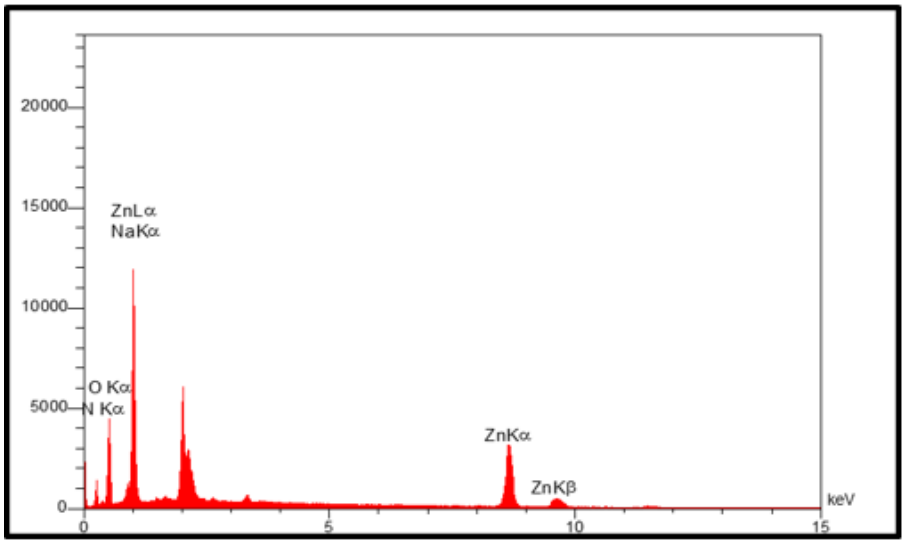

Figure 4) Elemental Composition and Distribution of ZnO Nanoparticles Analyzed by EDX

XRD Analysis:

Important information on the crystallographic arrangement of the zinc oxide nanoparticles (ZnO-NPs) was acquired by X-ray diffraction (XRD) analysis conducted at the XRD Laboratory of the University of Kashan, using a Copper (Cu) source. The diffraction pattern, recorded over a 2Theta range of 10° to 80°, exhibits prominent peaks at approximately 31.7°, 34.4°, 36.2°, 47.5°, 56.6°, 62.9°, 66.4°, 68.0°, and 69.1°. Referred to in file no. 36-1451 of the Joint Committee on Powder Diffraction Standards (JCPDS), these peaks correlate to the unique planes of hexagonal wurtzite ZnO crystals. Accurate confirmation of the successful production and purity of the ZnO-NPs is obtained by comparing these peaks with the standard ZnO diffraction pattern. Clearly defined diffraction peaks indicate a high level of crystallinity, consistent with the expected structural properties of ZnO nanoparticles. The verified X-ray diffraction (XRD) data verifies the effective synthesis of ZnO nanoparticles, following established worldwide scientific research criteria. The clearly distinguishable and well defined diffraction peaks ensure that the ZnO-NPs produced meet the expected criteria for generating nanoparticles of exceptional quality, making them suitable for various advanced applications in the domains of nanotechnology and materials science.

Trikkaliotis *et al.*,2020; Qayoom, and Dar, 2020.)

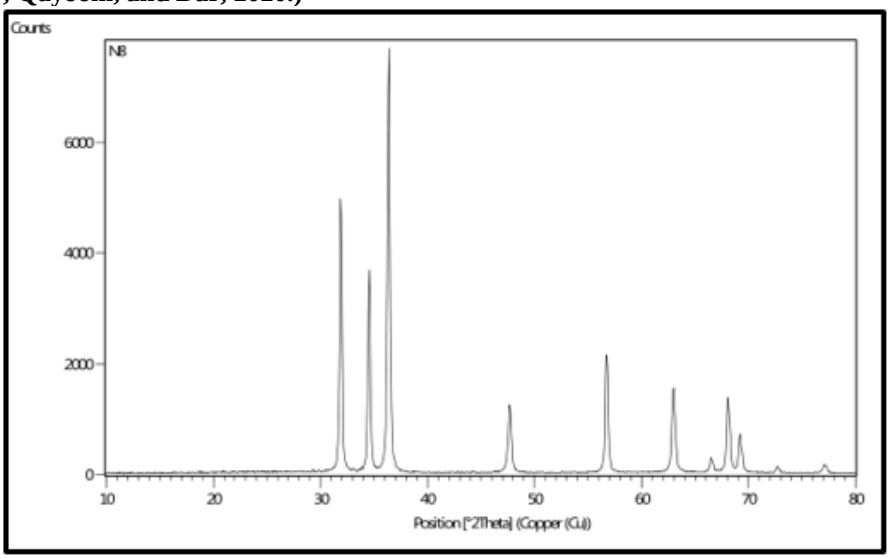

Figure 5) XRD Analysis

FTIR

Zinc oxide nanoparticles (ZnO-NPs) exhibit well defined absorption bands in their Fourier Transform Infrared (FTIR) spectra, which confirm the presence of various functional groups and the successful synthesis of ZnO nanoparticles. The wide band seen at around 3326.46 cm^{+1} in the first spectrum, 3288.48 cm^{+1} in the second spectrum, and 3348.91 cm^{+1} in the third spectrum are associated with the stretching vibrations of the O-H bond. These vibrations suggest the existence of hydroxyl groups or the absorption of water. The peaks seen at 2924.14 and 2850.99 cm^{+1} in the first spectrum, 2926.89 and 2863.95 cm^{+3} in the second spectrum, and 2926.89 and 2855.95 cm^{+3} in the third spectrum are ascribed to the stretching vibrations of C-H bonds, suggesting the existence of organic molecules. The prominent absorption bands seen at around 1619.38 cm^{+1} in the first spectrum and 1638.59 cm^{+1} in the second and third spectra are attributed to the stretching vibrations of C=O bonds, indicating the existence of carbonyl groups. The absorption band seen at around 1385.95 cm^{+3} (first and second spectra) and 1384.22 cm^{+3} (third spectrum) is specific to N-O stretching vibrations, which suggests the presence of nitrogen-containing chemicals. The detectable bands at around 875.74 cm^{+1} in all spectra offer dependable proof of the presence of Zn-O stretching vibrations, which are a distinctive property of zinc oxide nanoparticles. The FTIR spectra validate the successful synthesis of ZnO nanoparticles utilizing organic chemical constituents obtained from the biological extract used in the synthesis process. **Singh and Sharma, 2017.**

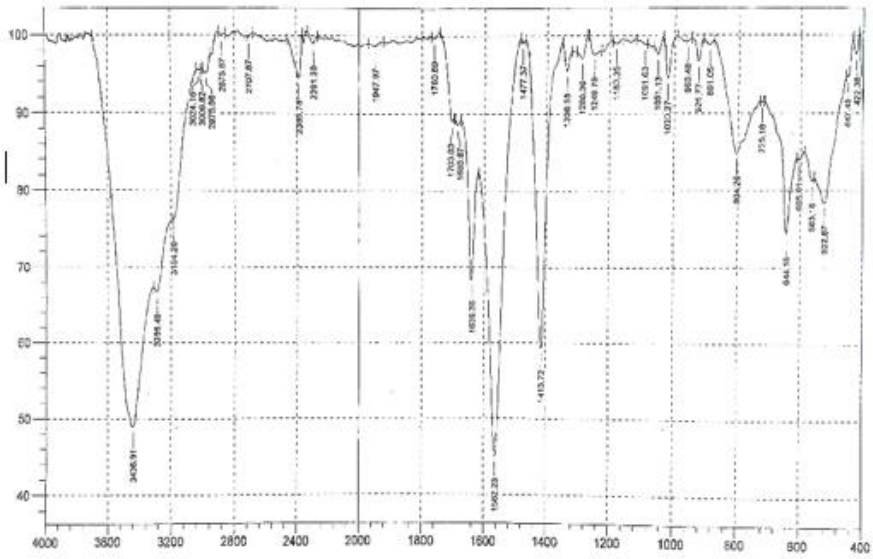

Figure 6): FTIR analysis of Extract.

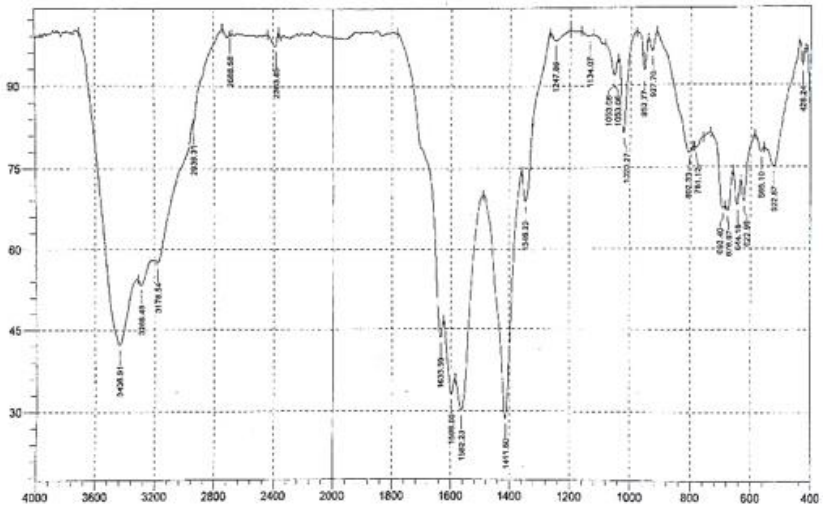

Figure 7). FTIR analysis of ZnO acetate.

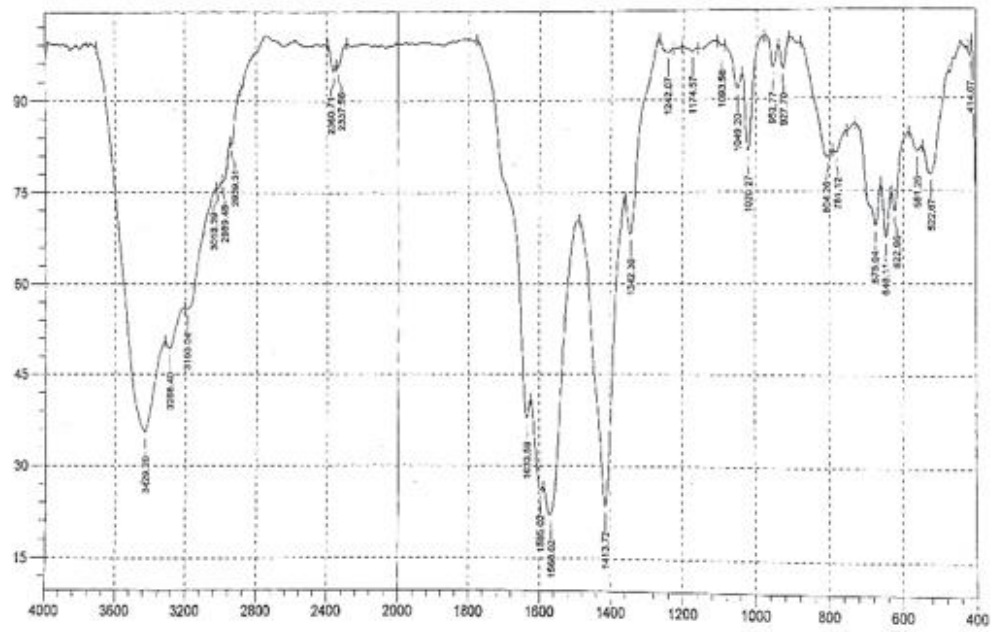

Figure 8). FTIR analysis of ZnO acetate +extract.

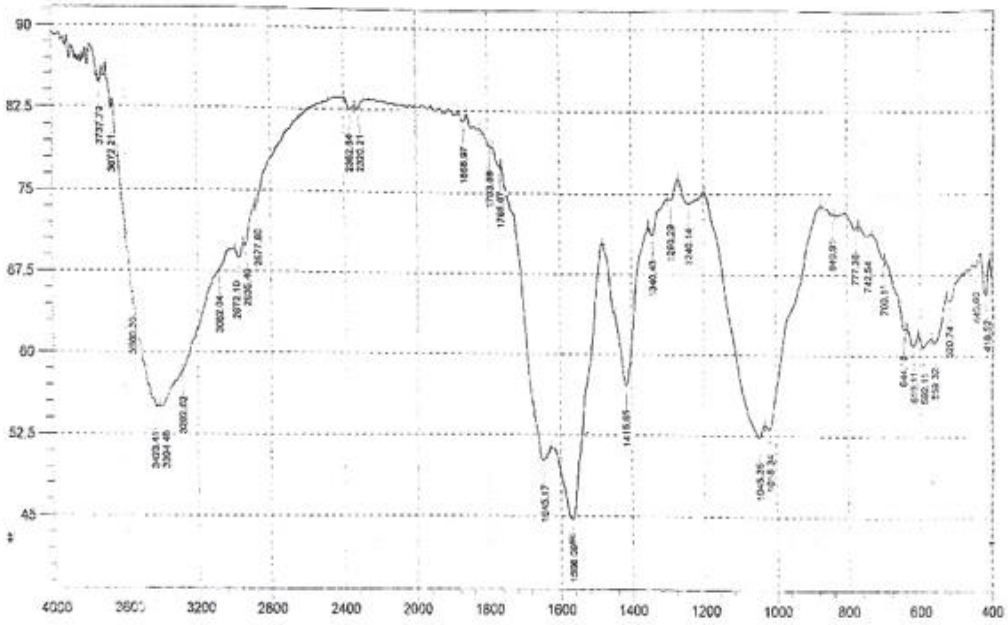

Figure 9). FTIR analysis of ZnO-NPS.

Immunological assay

In the immunological assay include TNF-a, post immunization notice the figure show The first group served as the control negative, which represents the baseline level in the absence of any treatment. The second and third group has high levels of TNF-α compared to first and fourth group that mean the exposure to sonication antigen or the combination of zinc oxide and sonication antigen (group ZnO) may lead to an increase in TNF-α. levels. Means that significantly higher than the other groups. The synergistic effect of the zinc oxide nanoparticles and the sonicated *S. lugdunensis* led to a much more pronounced inflammatory response, as indicated by the dramatically elevated TNF-α levels. The fourth group (S) was exposed to sonicated *Staphylococcus lugdunensis* alone. The high TNF-α level in this group suggests that the sonicated *S. lugdunensis* itself was capable of triggering a strong inflammatory response, as evidenced by the increased production of TNF-α.

The fourth group (ZnO)was exposed to zinc oxide nanoparticles, the increase in TNF-α level compared to the control negative group indicates that the zinc oxide nanoparticles triggered an inflammatory response, as evidenced by the elevated production of the pro-inflammatory cytokine TNF-α. While the result in the figure of post infection show This negative control group, representing the baseline TNF-α levels without any treatment. The second group serves as the positive control, representing the maximum TNF-α response without any

intervention. Third group received the sonicated antigen of *S. lugdunensis*, which induced a pro-inflammatory response. Beyond the first group but falling short of the second group.

Tumor necrosis factor-α (TNF-α) is involved in immune responses and inflammation. Through the interaction of bacterial components, such as cell wall components or toxins, with immune cells, Staphylococcus lugdunensis can induce the production of TNF-α. Thyrotropin-alpha (TNF-α) orchestrates the recruitment, activation, and development of inflammation in immune cells at the site of infection as a protective reaction against the bacteria. **(Koymans *et al*.,2017).** Evidence has demonstrated that Staphylococcus lugdunensis, a species belonging to the Staphylococcus genus, has the ability to engage with the immune system and regulate the production of certain immunological molecules like interleukin-10 (IL-10), tumor necrosis factor-alpha (TNF-α), and immunoglobulin G (IgG).**(Porcheron and Dozois, 2015).**

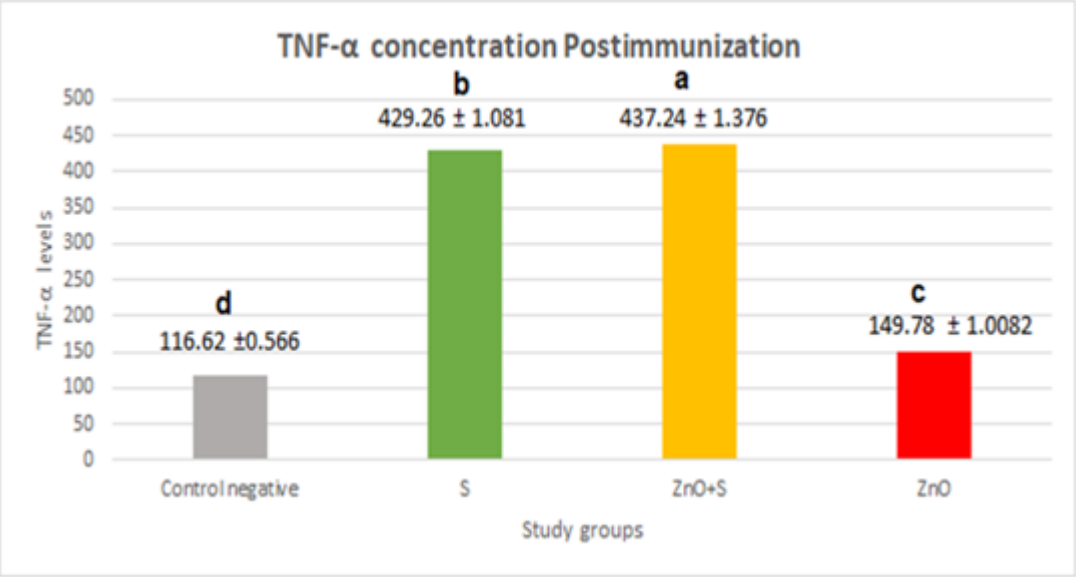

Figure 10) Serum TNF-a level in pg/ml as measured 28 days after immunization.

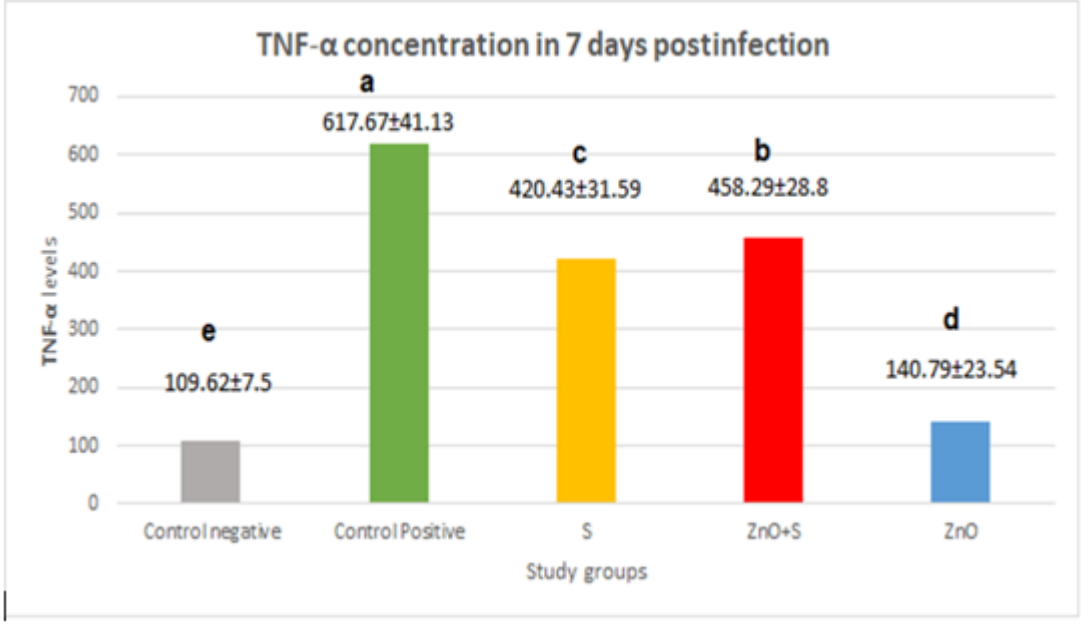

Figure 11) Level of serum TNF-a pg/ml (7-day post infection)

Histopathology examination

Histopathological section of the liver and the spleen at day 7 post infection

Histological examination at day 7 post infection in the positive control group revealed that liver showed disorganization of hepatic cord black arrow and MNCs infiltration in the portal area (figure12a), focal granulomatous in the liver parenchyma (figure 12b). While the spleen revealed mild hyperplasia of white pulp (figure 13a), severe destruction of splenic tissue characterized by hemorrhage and MNCs infiltration in right

pulp(figure13b), in other animal showed limited hyperplasia of the white pulp and significant damage to the splenic tissue marked by bleeding and infiltration of MNCs in the right pulp. (Sonicated S) group showed granulomatous lesion in the liver parenchyma (figure 14a), inflammatory cell mainly MNCs surrounding necrotic tissue (figure 14b). While the spleen showed normal spleen tissue (figure 15). The liver (sonicated S+ ZnO) group showed mild aggregation of MNCs in liver parenchyma (figure 16a), and mild fatty changes in the hepatocytes (figure16 b). While the spleen showed mild hyperplasia of the white pulp (figure 17).

Histopathological section of the liver and the spleen at day 21 post infection

Histological examination at day 21 post infection in the positive control group that the liver showed Hepatocyte Fatty change (figure 18a), necrosis of the hepatocytes (figure 18b), mild MNCs infiltration with the portal area (figure 18c), thrombus detected in the portal region (figure 18d). While the spleen revealed depletion of white pulp and congestion of blood vessels (figure 19). The liver of (Sonicated S) group showed necrotic changes of hepatocytes and MNCs in the liver parenchyma (figure 20a), mild MNCs infiltration in the portal area (figure 20b). While the spleen showed normal section (figure 21). The liver of (Sonicated S+ ZnO) group showed dilation of central vein (figure 22a), focal aggregation of MNCs (figure 22 b). While the spleen showed mild hyperplasia of white pulp (figure 23).

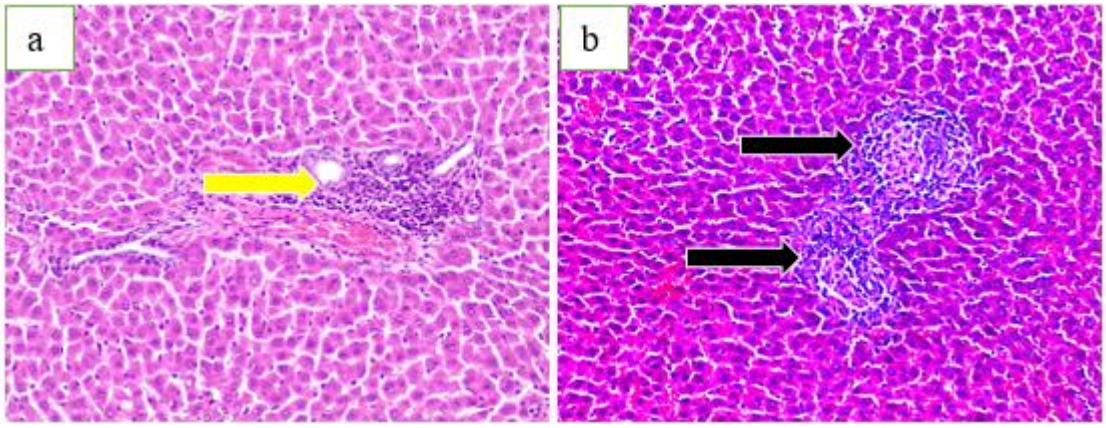

Figure 12) Histopathological section in the liver **(control positive)** group day 7 post infection showed (a) disorganization of hepatic cord black arrow and MNCs infiltration in the portal Region yellow arrow (H and E stain 20X) (b) focal granulomatous within the liver parenchyma black arrow (H and E stain 100X

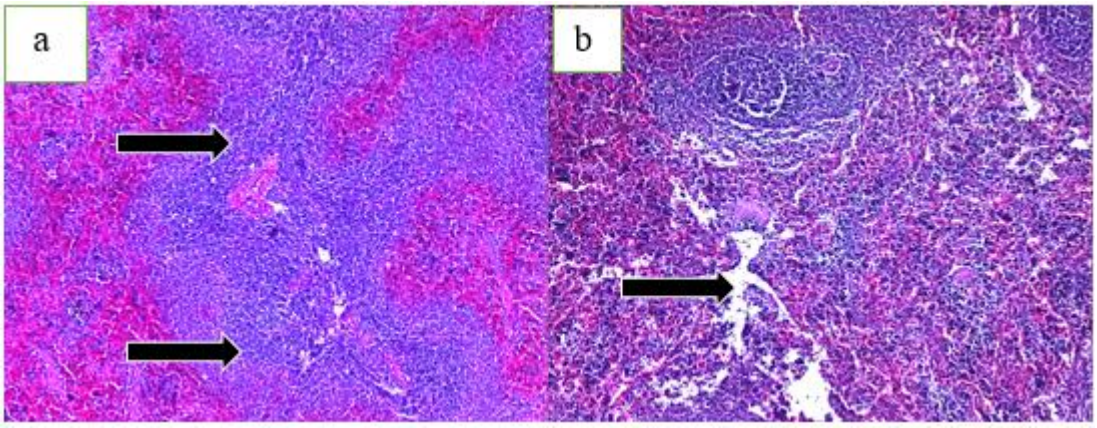

Figure 13) Histopathological section within the spleen **(control positive)** group day 7 post infection showed (a) mild hyperplasia of white pulp (40X) (b) severe destruction of splenic tissue characterized by hemorrhage and MNCs infiltration in right pulp black arrow (40X).

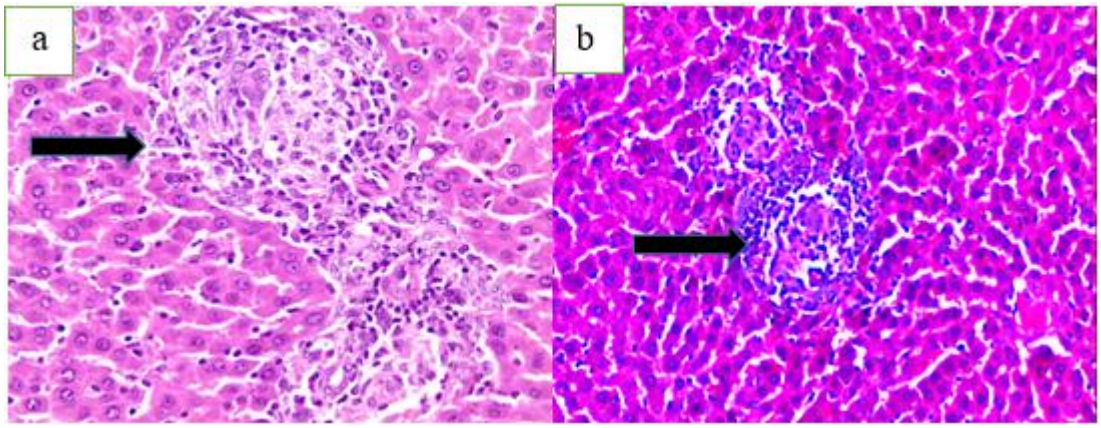

F**igure 14)** Histopathological section in the liver (**sonicated S)** group day 7 post infection showed (a) granulomatous lesion in the liver parenchyma black arrow (40X). (b) inflammatory cell mainly MNCs surrounding necrotic tissue black arrow (100X)

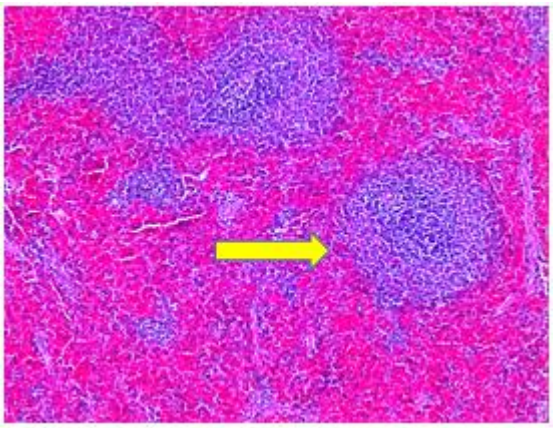

Figure 15) Histopathological section in the spleen **(sonicated S)** group day 7 post infection showed normal spleen (H and E stain 40X

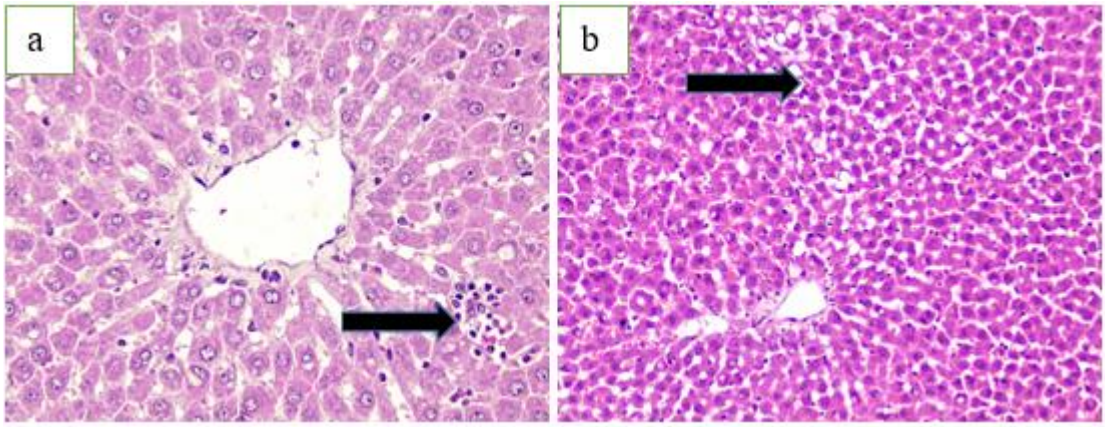

Figure 16) Histopathological section in the liver **(sonicated S+ ZnO)** group day 7 post infection showed (a) mild aggregation of MNCs in liver parenchyma (40X). (b) mild fatty changes in the hepatocytes (20X).

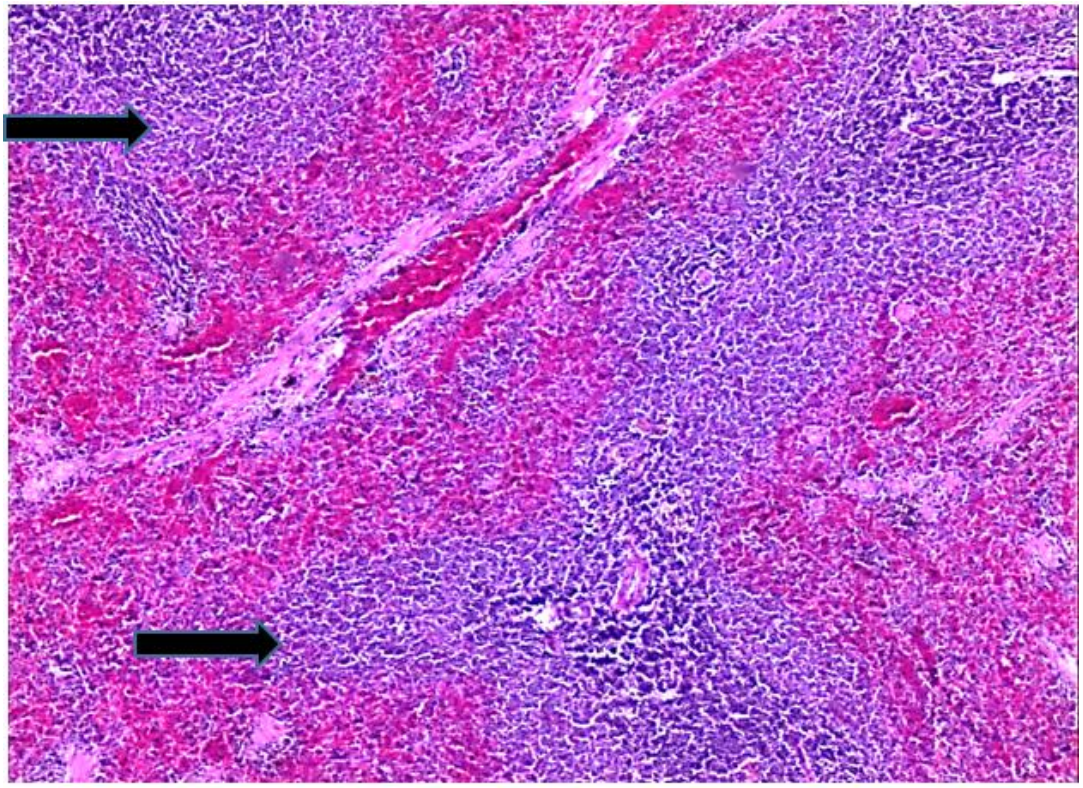

Figure 17) Histopathological section in the spleen (**sonicated S+ ZnO)** group day 7 post infection showed mild hyperplasia of the white pulp black arrow (H and E stain 40X

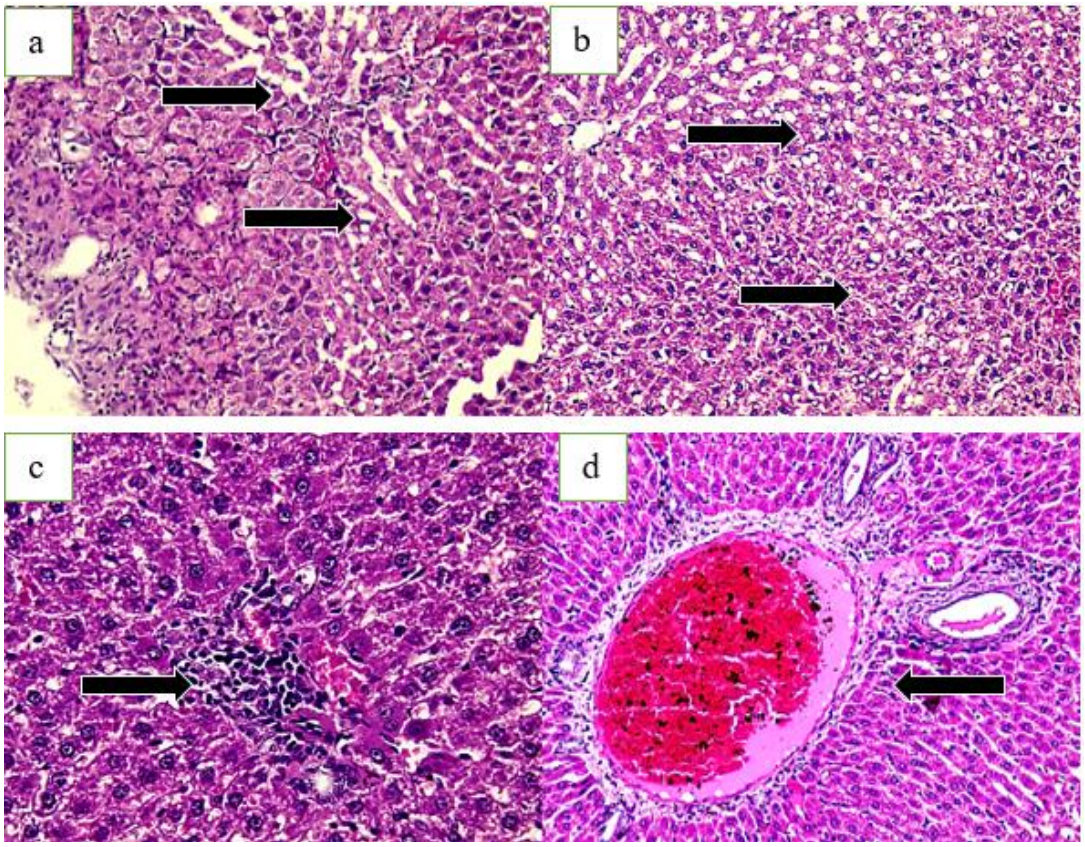

Figure 18) Histopathological section in the liver of (**control positive)** group day 21 post infection showed (a) Hepatocyte Fatty change black arrow (100X) (b) necrosis of the hepatocytes black arrow (100X). (c) mild MNCs infiltration in the portal area black arrow (100X). (d) Thrombus in the portal area black arrow (100X).

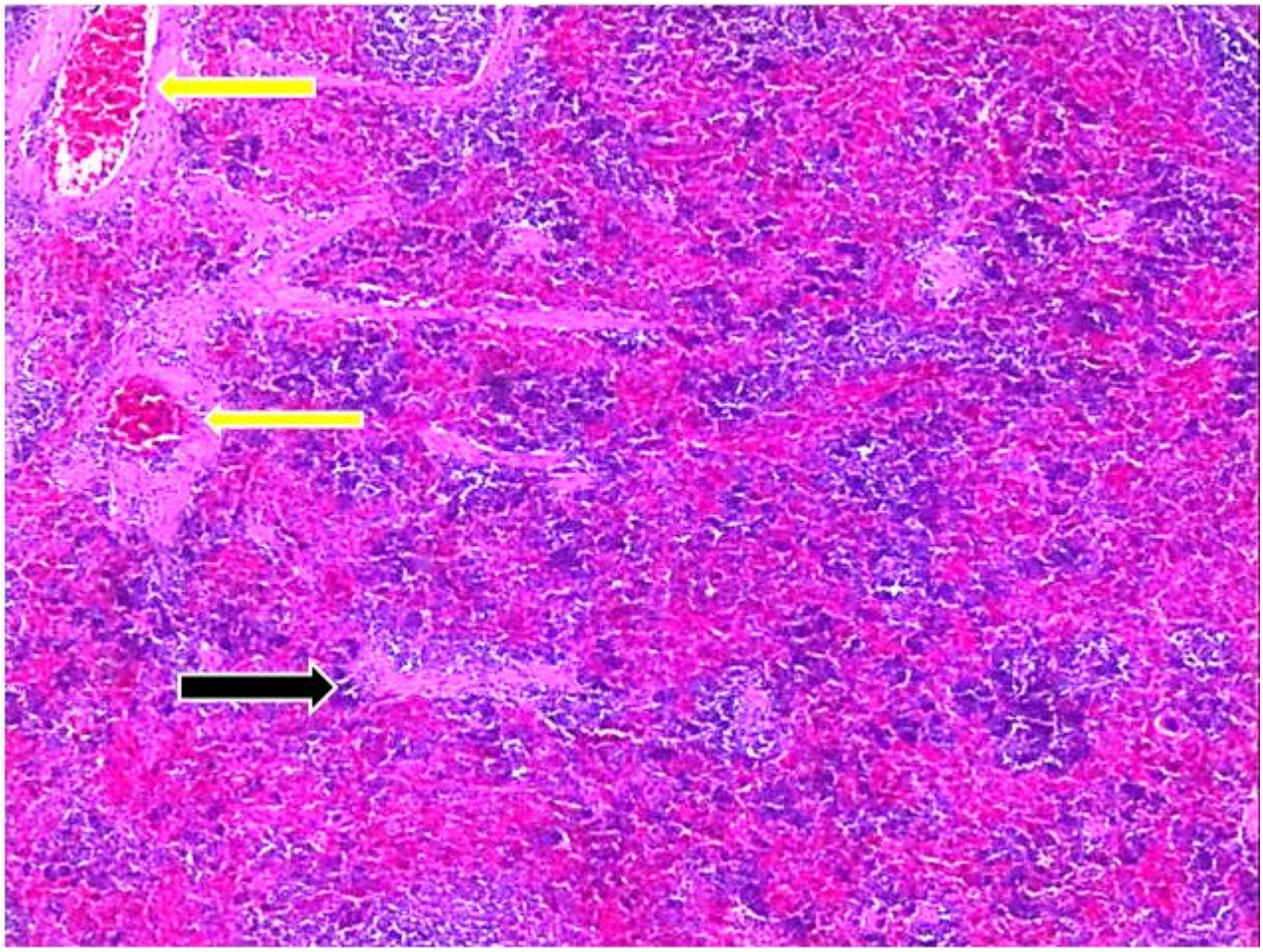

Figure19) Histopathological section in the spleen (**control positive)** group day 21 post infection showed depletion of white pulp black arrow and congestion of blood vessels yellow arrow (H and E stain 40X

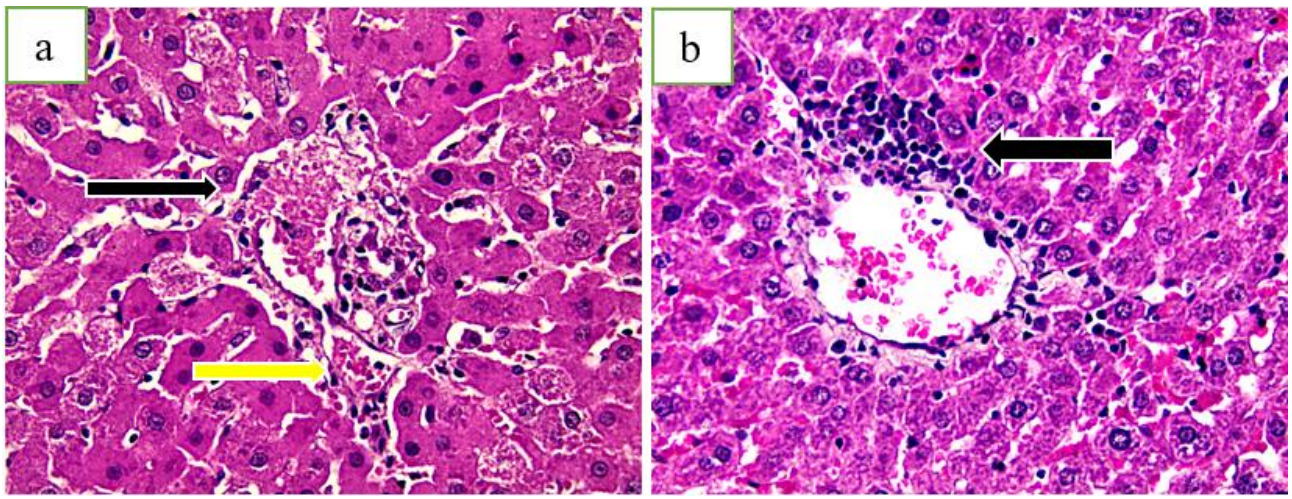

Figure 20) Histopathological section in the liver of (**Sonicated S)** group day 21 post infection showed (a) necrotic changes of hepatocytes black arrow and MNCs in the liver parenchyma yellow arrow (100X). (b) mild MNCs infiltration in the portal area black arrow (100X).

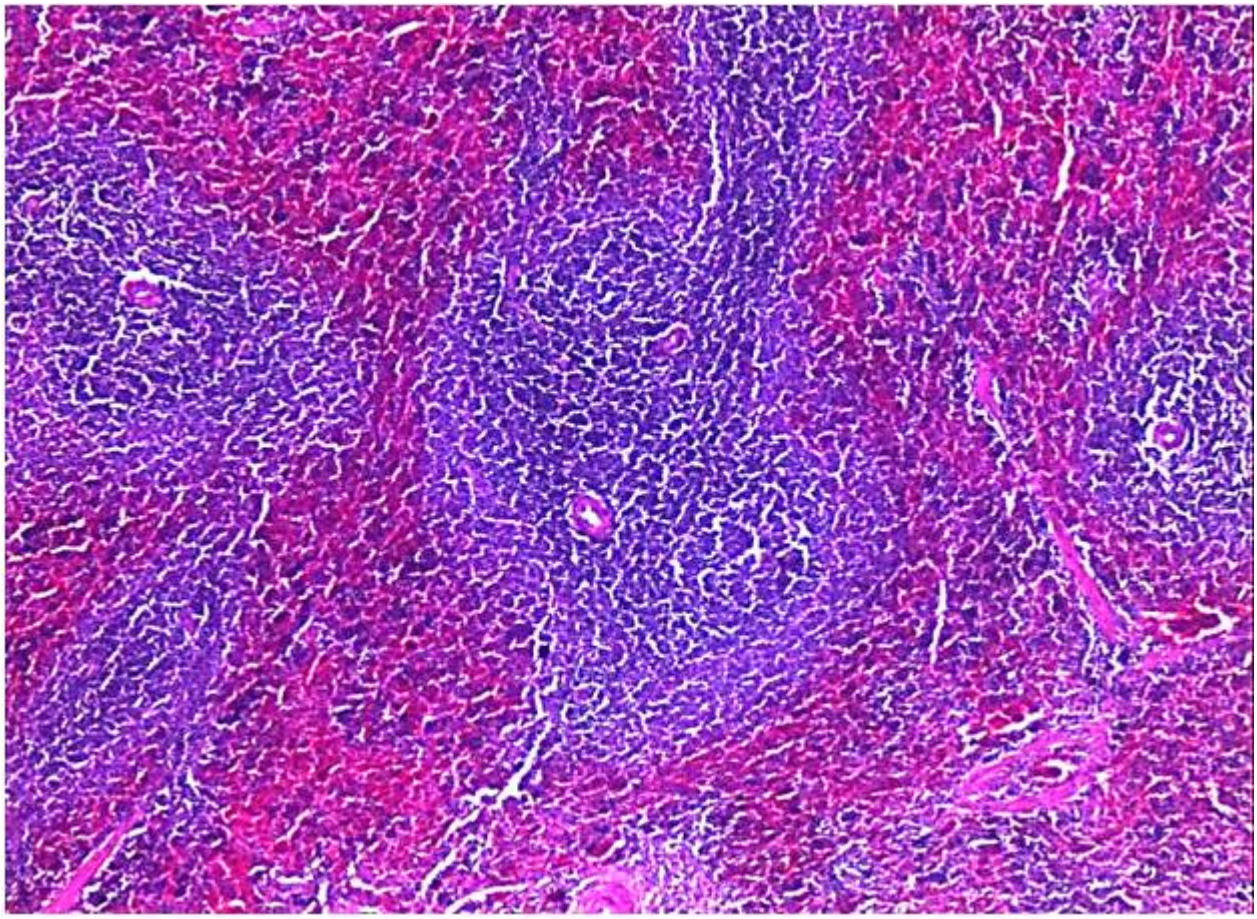

Figure21) Histopathological section in the spleen (**Sonicated S)** group day 21 post infection showed normal section (H and E stain 40X

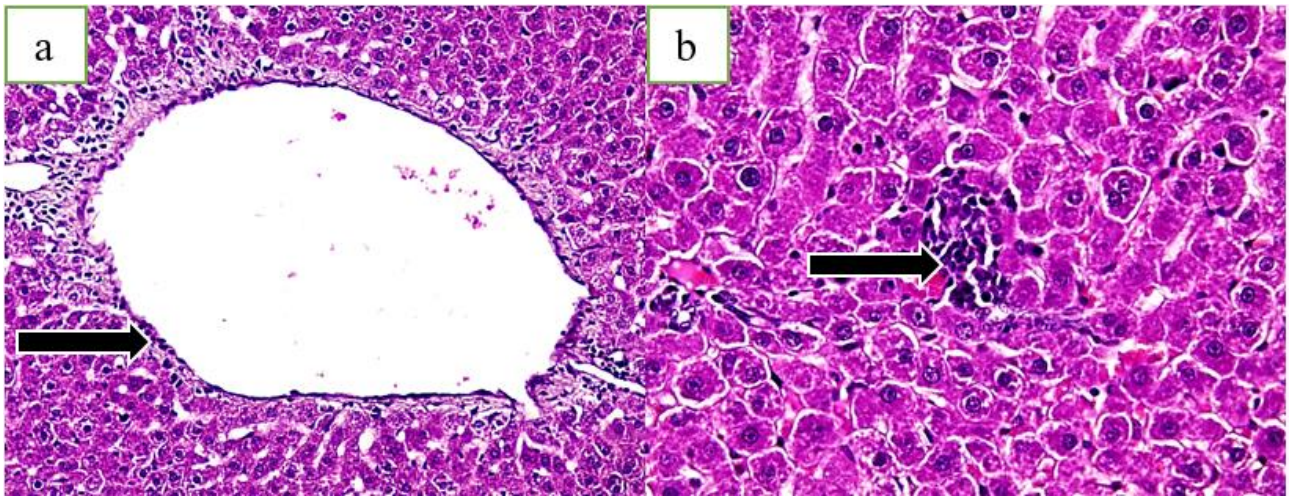

Figure 22) Histopathological section in the liver of (**Sonicated S+ ZnO)** group day 21 post infection showed (a) dilation of central vein black arrow (100X) (b) Focal aggregation of MNCs black arrow (100X).

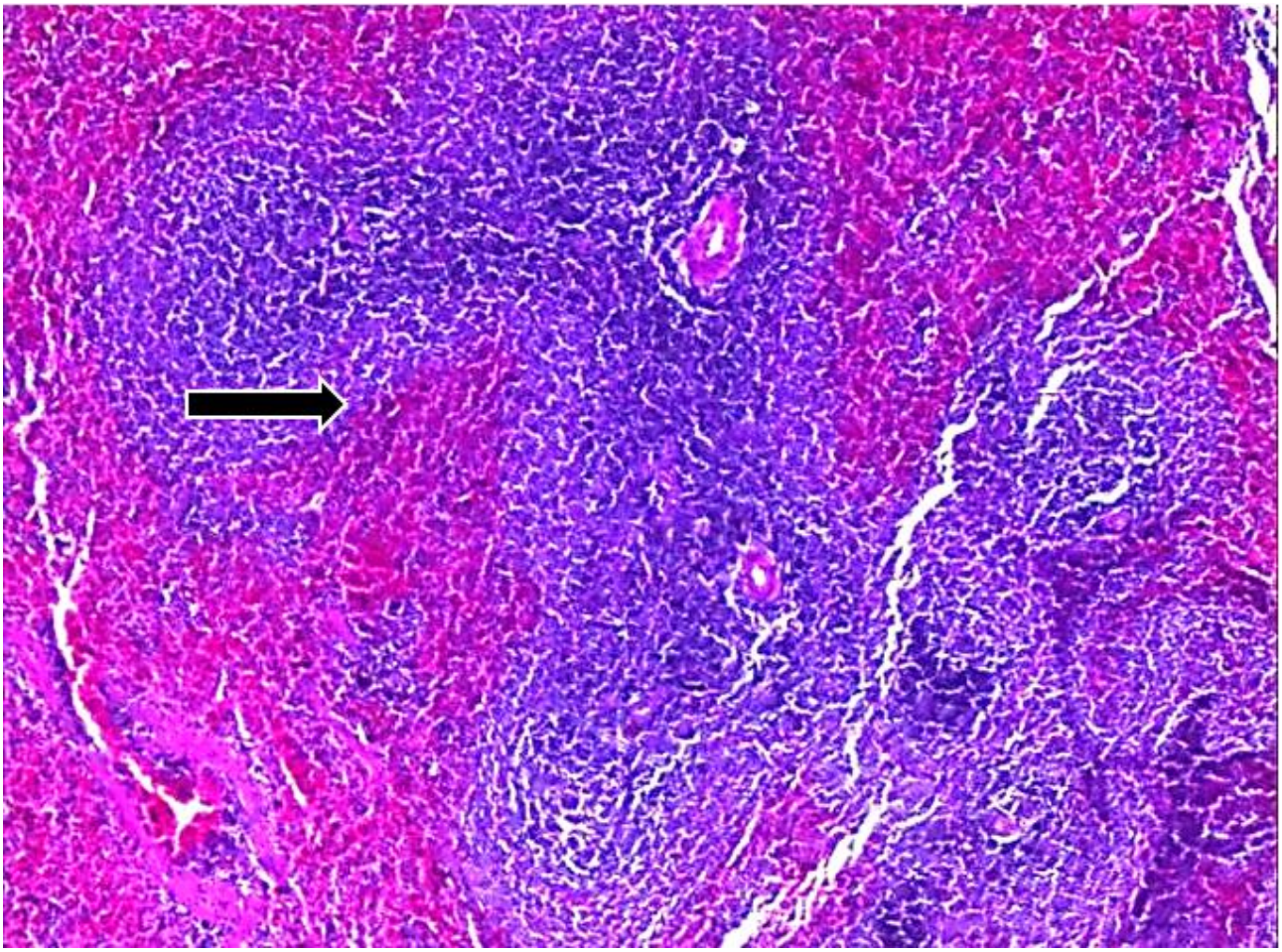

Figure 23) Histopathological section in the spleen of (**Sonicated S+ ZnO)** group day 21 post infection showed mild hyperplasia of white pulp black arrow (H and E stain 40X

Discussion

Plant-derived nanoparticles are gaining recognition as promising adjuvants in vaccine development due to their biocompatibility, low toxicity, and capacity to enhance immune responses. These nanoparticles can be used to boost the efficacy of vaccines by enhancing the body's immune response to the antigen, ensuring that a more robust and long-lasting immunity is achieved. The main aim of this study was to evaluate the ability of plant-derived nanoparticles to enhance immunoactivity when in combination with sonicated *S. lugdunensis* bacteria. Zinc oxide nanoparticles (NPs) have been demonstrated to trigger the production and release of certain pro-inflammatory cytokines, such as tumor necrosis factor-alpha (TNF-α), interleukin-6 (IL-6), and interleukin-8 (IL-8), by various populations of immune cells. **(Wahab *et al.*,2014; Kaushik *et al.*, 2015; Pandurangan *et al.*,2015).** As well as can act as adjuvants, enhancing the uptake of antigens by antigen-presenting cells (APCs) like dendritic cells, leading to improved T-cell activation, which are crucial for adaptive immunity, and the phagocytic activity of macrophages cam improved by ZnO-NPS that lead to clearance of pathogens **Sherif *et al.*, 2023).**

○ The main role of dendritic cells is to stimulate and regulate immune responses by presenting antigens to other immune cells and release pro-inflammatory cytokines, including tumor necrosis factor-alpha (TNF-α) **(Kang *et al.*,2013).** The maturation of DCs by ZnO NPs stimulation, lead to increase the expression of co-stimulatory molecules such as CD80, CD86 and major histocompatibility complex (MHC) molecules, which are essential for effective T-cell activation as well as the ability of DCs to present antigens in a more effective manner improves T-cell activation and subsequently helps in B-cell activation, differentiation, and antibody production through T-cell help **Lee *et al.*,2023).**

Detection of *S. lugdunensis* and its pathogenic components in the liver can trigger an immune response characterized by inflammation. During the immunological response, immune cells are recruited and activated, leading to the release of pro-inflammatory cytokines and causing damage to certain organs. Successful evasion of innate immune responses is critical for the survival of a pathogen that causes invasive infections. Several proteins of Staphylococcus aureus interfere with the activation and migration of neutrophils in response to the host. and Bacterial chemotactic agents induce neutrophil lysis and degradation of neutrophil extracellular traps, disrupt opsonization, opsonin, and neutrophil phagocytosis, and enhance bacterial survival within the neutrophil membrane. **(Spaan *et al.*, 2017; Rooijakkers and van Strijp, 2007).** Several molecular processes can elucidate the advantageous impact of such nanoparticles as adjuvants. One approach involves the functionalization of plant-derived nanoparticles

with antigens or other immunostimulatory molecules. Upon introduction into the body, these nanoparticles rapidly undergo uptake by antigen-presenting cells (APCs) including dendritic cells and macrophages. The second mechanism is Within antigen-presenting cells (APCs), nanoparticles facilitate the efficient processing and presentation of antigens on major histocompatibility complex (MHC) molecules. Optimal presentation is crucial for the stimulation of T-cells, which are essential for both the commencement of the immune response and the following generation of antibodies by B-cells. The sonicated antigen of *Staphylococcus lugdunensis* can trigger both the innate and adaptive immune systems. the current study has shown that the sonicated antigen Ags can stimulate the innate immune response, namely by being recognized by pattern recognition receptors (PRRs) and triggering inflammatory pathways downstream. **(Heilbronner *et al.*, 2011).** Moreover, it has been demonstrated to trigger an adaptive immunological response, resulting in the stimulation of T cells and B cells to generate antibodies. **(Becker *et al*.,2014; Zipperer *et al.*, 2016).** Activation of helper T cells (CD4+ T cells) occurs when they identify the antigen-MHC complex on dendritic cells. cytokines secrete by T lymphocytes cell that have activated and influence and modify the immune response. **(Joffre *et al*.,2012).**

These findings revealed that the co-administration of zinc oxide nanoparticle and sonication antigen can significantly enhance the production of TNF-a compared to the individual exposure to zinc oxide alone (ZnO group).

The boom in TNF-a ranges suggests an immune reaction and ability activation of inflammatory pathways inside the rats' blood following immunization. The distinct experimental settings, as well as the duration of vaccination and the quantity of materials employed, are crucial factors that will influence the reported variations in TNF-a stages. Furthermore, the substantial increase in TNF-a levels seen in the group treated with the combination of zinc oxide and sonication antigen indicates a potential synergistic effect between these components. Furthermore, zinc oxide can serve as an adjuvant in this combination. Hence, it is plausible that zinc oxide, when used as an adjuvant, amplifies the stimulation of dendritic cells and finally augments the synthesis of TNF-a in reaction to the sonication antigen. **(Shang *et al*.,2014).** Furthermore, this combination may also result in an enhanced immunological response, leading to the observed increase in TNF-a levels in the ZnO group. In the bacteria Staphylococcus lugdunensis, the presence of the Fbl gene, also known as the fibrinogen-binding protein gene, leads to the buildup of liver thrombus. The function of this gene is to encode a protein that is involved in the bacterium's interaction with fibrinogen, a protein present in the blood plasma. **Argemi *et al*.,2019).**

An investigation was conducted to determine the functional role of the Fbl gene in the development of infections caused by Staphylococcus lugdunensis. Fibrinogen-binding proteins have a substantial impact on the attachment of Staphylococcus lugdunensis to host tissues and the proliferation of biofilms, which can prolong and worsen infections. **Argemi *et al*.,2018).** Previous research on infectious bacteremia has resulted in the development of the neutrophil extracellular trap (NET) theoretical frame work. **(Wartha *et al.*, 2007).** Pathogen spread often occurs accompanying infectious bacteremia. **(Moreillon *et al.*, 2002).** Platelets inhibit the transmission of diseases by their interaction with infectious agents, promoting the formation of blood clots, and creating neutrophil extracellular traps (NETs), which have been demonstrated to stop the progression of infections. **(Jung *et al.*, 2015).**

The liver granulomatous lesions demonstrate that the immune system in rats elicits a restricted, granulomatous reaction to Staphylococcus lugdunensis infection in the liver. **(Nishina *et al.*, 1997).** Infection with Staphylococcus lugdunensis in rats has been found to be associated with the formation of granulomatous lesions in the liver, most likely triggered by the host's immune response **(Missiaggia *et al.*, 2021).** These aggregate of mononuclear cells reveal an effort by the host's immune system to limit and eliminate the bacterial infection in the liver (**Seifi *et al.*, 2020).**

A study by **Li *et al.*,2020)** Identification of minor aggregation or infiltration of mononuclear cells, such as lymphocytes and monocytes, in the hepatic tissue of rats affected by Staphylococcus lugdunensis. Furthermore, it was shown that the accumulation of lipids inside the hepatocytes resulted in further deterioration of liver function and heightened susceptibility of the liver to further injury. **(Chen *et al.*, 2022).** The researchers also observed a correspondence between the degree of hepatocyte necrosis and the bacterial load, where higher levels of infection led to a more extensive cell death (**Wang *et al.*, 2021**). The liver demonstrated an inflammatory reaction as a mechanism to delimit and eradicate the bacterial infection. Yet, the presence of these mononuclear cells disrupted the typical architectural arrangement of the liver. Furthermore, a modest buildup of mononuclear cells, such as lymphocytes and monocytes, was seen in the liver tissue of rats challenged with Staphylococcus lugdunensis **(Zheng *et al.*, 2018).**

Conclusion, the use of sonicated *Staphylococcus lugdunensis* Antigens (sonicated Ags) can effectively activate the immune system and offer limited defense against *S. lugdunensis* infection, particularly when combined with zinc oxide nanoparticles. That lead This study could be first step for (foundation step) studying the pathogenesis and developing vaccination for animals in future studies

Reference

Bieber L, Kahlmeter G. Staphylococcus lugdunensis in several niches of the normal skin flora. Infect Dis. 2010;16:385-8.

Frank KL, Del Pozo JL, Patel R. From clinical microbiology to infection pathogenesis: how daring to be different works for Staphylococcus lugdunensis. Clin Microbiol Rev. 2008;21(1):111-33. doi: 10.1128/CMR.00036-07.

Argemi X, Prevost G, Riegel P, Provot C, Badel-Berchoux S, Jehl F, et al. Kinetics of biofilm formation by Staphylococcus lugdunensis strains in bone and joint infections. Diagn Microbiol Infect Dis. 2017;88(4):298-304. doi: 10.1016/j.diagmicrobio.2017.06.012.

Non LR, Santos CAQ. The occurrence of infective endocarditis with Staphylococcus lugdunensis bacteremia: a retrospective cohort study and systematic review. J Infect. 2017;74(2):179-86. doi: 10.1016/j.jinf.2016.10.003.

Papapetropoulos N, Papapetropoulou M, Vantarakis A. Abscesses and wound infections due to Staphylococcus

lugdunensis: report of 16 cases. Infection. 2013;41(3):525-8. doi: 10.1007/s15010-012-0381-z.

Mitchell J, Tristan A, Foster TJ. Characterization of the fibrinogen-binding surface protein Fbl of *Staphylococcus lugdunensis*. Microbiology. 2004;150(11):3831-3841. doi: 10.1099/mic.0.27337-0.

Nilsson M, Bjerketorp J, Wiebensjö Å, Ljungh Å, Frykberg L, Guss B. A von Willebrand factor-binding protein from *Staphylococcus lugdunensis*. FEMS Microbiol Lett. 2004;234(1):155-161. doi: 10.1111/j.1574-6968.2004.tb09527.x.

Nilsson M, Bjerketorp J, Guss B, Frykberg L. A fibrinogen-binding protein of *Staphylococcus lugdunensis*. FEMS Microbiol Lett. 2004;241(1):87-93. doi: 10.1016/j.femsle.2004.10.008.

Heilbronner S, Monk IR, Brozyna JR, Heinrichs DE, Skaar EP, Peschel A, et al. Competing for iron: duplication and amplification of the isd locus in *Staphylococcus lugdunensis* HKU09-01 provides a competitive advantage to overcome nutritional limitation. PLoS Genet. 2016;12(4):e1006246. doi: 10.1371/journal.pgen.1006246.

Rook KA, Brown DC, Rankin SC, Morris DO. Case–control study of *Staphylococcus lugdunensis* infection isolates from small companion animals. Vet Dermatol. 2012;23(6):476-e90. doi: 10.1111/j.1365-3164.2012.01070.x.

Rozalska B, Ljungh A: 1995, Biomaterial-associated staphylococcal peritoneal infections in a neutropaenic mouse model. FEMS Immunol Med Microbiol 11:307–319.

Gahukamble AD, McDowell A, Post V, Ehricht R, Monecke S, Wagner K, et al. *Propionibacterium acnes* and *Staphylococcus lugdunensis* cause pyogenic osteomyelitis in an intramedullary nail model in rabbits. J Clin Microbiol. 2014;52(5):1595-1606. doi: 10.1128/JCM.00465-

Zbinden R, Müller F, Brun F, von Graevenitz A. Detection of clumping factor-positive *Staphylococcus lugdunensis* by Staphaurex Plus®. J Microbiol Methods. 1997;31(1-2):95-98. doi: 10.1016/S0167-7012(97)00062-5.

Kalpana VN, Devi Rajeswari V. A review on green synthesis, biomedical applications, and toxicity studies of ZnO NPs. Bioinorganic chemistry and applications. 2018;2018(1):3569758. (https://doi.org/10.1155/2018/3569758).

Siddiqi KS, Rahman AU, Tajuddin, Husen A. Properties of Zinc Oxide Nanoparticles and Their Activity Against Microbes. *Nanoscale Res Lett*. 2018;13:141. doi: [10.1186/s11671-018-2532-3](https://doi.org/10.1186/s11671-018-2532-3).

Aadim KA, Abbas IK. Synthesis and Investigation of the Structural Characteristics of Zinc Oxide Nanoparticles Produced by an Atmospheric Plasma Jet. *Iraqi J Sci*. 2023; pp.1743-1752. doi: [10.24996/ijs.2023.64.4.5](https://doi.org/10.24996/ijs.2023.64.4.5).

Khitam SS, Alhtheal ED, Azhar JB. Effect of zinc oxide nanoparticles preparation from zinc sulphate (ZnSO4) against gram-negative or gram-positive microorganisms in vitro. *Iraqi J Sci*. 2018.

Al-Hraishawi H, Al-Saadi N, Jabbar S. In Vitro Analysis: The Anticancer Activity of Zinc Oxide Nanoparticles from Cinnamomum Verum. *J Nanostructures*. 2023;13(1):146-150. doi: [10.22052/JNS.2023.01.017](https://doi.org/10.22052/JNS.2023.01.017).

Husain WM, Araak JK, Ibrahim OM. Green synthesis of zinc oxide nanoparticles from (Punica granatum L) pomegranate aqueous peel extract. *Iraqi J Vet Med*. 2019;43(2):6-14. doi: [10.30539/iraqijvm.v43i2.287](https://doi.org/10.30539/iraqijvm.v43i2.287).

Yusof HM, Mohamad R, Zaidan UH, Rahman NAA. Microbial synthesis of zinc oxide nanoparticles and their potential application as an antimicrobial agent and a feed supplement in animal industry: A review. *J Anim Sci Biotechnol*. 2019;10:57. doi: [10.1186/s40104-019-0368-z](https://doi.org/10.1186/s40104-019-0368-z).

Alwash A. The green synthesis of zinc oxide catalyst using pomegranate peels extract for the photocatalytic degradation of methylene blue dye. *Baghdad Sci J*. 2020;17(3):0787-0787. doi: [10.21123/bsj.2020.17.3.0787](https://doi.org/10.21123/bsj.2020.17.3.0787).

Al-Ghareebawi AM, Al-Okaily BN, Ibrahim OMS. Characterization of zinc oxide nanoparticles synthesized by olea europaea leaves extract (part L). *Iraqi J Agric Sci*. 2021;52(3):580-588. doi: [10.36103/ijas.v52i3.1406](https://doi.org/10.36103/ijas.v52i3.1406).

Majeed SM, Ahmed ME, Ali IA. Comparison of Sizes of Zinc Oxide Nanoparticles Extracted from *Staphylococcus lugdunensis* and *Berberis vulgaris* Plant Extract Against Some Types of Bacteria and Yeast. *J Drug Deliv Technol*. 2022;12(1):103-107.

Mohammed NI, Alwan MJ. Influence immunization by culture filtrate *Staphylococcus aureus* antigen carried by silver nanoparticles as adjuvant against *Staphylococcus aureus* infection in mice. Int J Sci Nat. 2017;8(3):695-703.

Malekshah RE, Shakeri F, Aallaei M, Hemati M, Khaleghian A. Biological evaluation, proposed molecular mechanism through docking and molecular dynamic simulation of derivatives of chitosan. Int J Biol Macromol. 2021;166:948-66. doi: 10.1016/j.ijbiomac.2020.10.230.

Hernández-Aguirre OA, Nunez-Pineda A, Tapia-Tapia M, Gomez Espinosa RM. Surface modification of polypropylene membrane using biopolymers with potential applications for metal ion removal. J Chem. 2016;2016:1-8. doi: 10.1155/2016/5163187.

Patel SR, Patel MP. Green and facile preparation of ultrasonic wave-assisted chitosan-g-poly-(AA/DAMPB)/Fe3O4 composite hydrogel for sequestration of reactive black 5 dye. Polymer Bull. 2021:1-25. doi: 10.1007/s00289-021-03557-8.

Zabihi E, Babaei A, Shahrampour D, Arab-Bafrani Z, Mirshahidi KS, Majidi HJ. Facile and rapid in-situ synthesis of chitosan-ZnO nano-hybrids applicable in medical purposes; a novel combination of biomineralization, ultrasound, and bio-safe morphology-conducting agent. Int J Biol Macromol. 2019;131:107-16. doi: 10.1016/j.ijbiomac.2019.03.073.

Trikkaliotis DG, Christoforidis AK, Mitropoulos AC, Kyzas GZ. Adsorption of copper ions onto chitosan/poly(vinyl alcohol) beads functionalized with poly(ethylene glycol).

Carbohydr Polym. 2020;234:115890. doi: 10.1016/j.carbpol.2020.115890.

Qayoom M, Dar GN. Crystallite size and compressive lattice strain in $NiFe_2O_4$ nanoparticles as calculated in terms of various models: influence of annealing temperature. Int J Self-Propag High-Temp Synth. 2020;29:213-219. doi: 10.3103/S106138622004005X.

Singh AP, Sharma RK. Selective sorption of Fe (II) ions over Cu (II) and Cr (VI) ions by cross-linked graft copolymers of chitosan with acrylic acid and binary vinyl monomer mixtures. Int J Biol Macromol. 2017;105:1202-1212. doi: 10.1016/j.ijbiomac.2017.07.004.

Koymans KJ, Vrieling M, Gorham RD, van Strijp JA. Staphylococcal immune evasion proteins: structure, function, and host adaptation. In: *Staphylococcus aureus*: Microbiology, Pathology, Immunology, Therapy and Prophylaxis. 2017. p. 441-489. doi: 10.1007/978-3-319-53165-1_14.

Porcheron, G. and Dozois, C.M., 2015. Interplay between iron homeostasis and virulence: Fur and RyhB as major regulators of bacterial pathogenicity. *Veterinary microbiology*, *179*(1-2), pp.2-14

Wahab R, Siddiqui MA, Saquib Q, Dwivedi S, Ahmad J, Musarrat J, Al-Khedhairy AA. ZnO nanoparticles induced oxidative stress and apoptosis in HepG2 and MCF-7 cancer cells and their antibacterial activity. Colloids Surf B Biointerfaces. 2014;117:267-276. doi: 10.1016/j.colsurfb.2014.02.038.

Kaushik N, Uddin N, Sim GB, Hong YJ, Baik KY, Kim CH, Choi EH. Responses of solid tumor cells in DMEM to reactive oxygen species generated by non-thermal plasma and chemically induced ROS systems. Sci Rep. 2015;5(1):8587. doi: 10.1038/srep08587.

Pandurangan M, Veerappan M, Kim DH. Cytotoxicity of zinc oxide nanoparticles on antioxidant enzyme activities and mRNA expression in the cocultured C2C12 and 3T3-L1 cells. Appl Biochem Biotechnol. 2015;175:1270-1280. doi: 10.1007/s12010-014-1375-4.

Sherif, A.H., Abdelsalam, M., Ali, N.G. and Mahrous, K.F., 2023. Zinc oxide nanoparticles boost the immune responses in Oreochromis niloticus and improve disease resistance to Aeromonas hydrophila infection. *Biological Trace Element Research*, *201*(2), pp.927-936.

Kang T, Guan R, Chen X, Song Y, Jiang H, Zhao J. In vitro toxicity of different-sized ZnO nanoparticles in Caco-2 cells. Nanoscale Res Lett. 2013;8(1):93. doi: 10.1186/1556-276X-8-93.

Lee S, Kim J, Park H, Chen X, Nguyen T. Mechanisms of dendritic cell activation by zinc oxide nanoparticles: implications for vaccine development. J Nanobiotechnol. 2023;21(1):45-57.

Spaan AN, van Strijp JA, Torres VJ. Leukocidins: staphylococcal bi-component pore-forming toxins find their receptors. Nat Rev Microbiol. 2017;15(7):435-447. doi: 10.1038/nrmicro.2017.27.

Rooijakkers SH, van Strijp JA. Bacterial complement evasion. Mol Immunol. 2007;44(1-3):23-32. doi: 10.1016/j.molimm.2006.06.011.

Heilbronner S, Foster TJ. *Staphylococcus lugdunensis*: a skin commensal with invasive pathogenic potential. Clin Microbiol Rev. 2021;34(1):e00205-20. doi: 10.1128/CMR.00205-20.

Becker K, Heilmann C, Peters G. Coagulase-negative staphylococci. Clin Microbiol Rev. 2014;27(4):870-926. doi: 10.1128/CMR.00109-13.

Zipperer A, Konnerth MC, Laux C, Berscheid A, Janek D, Weidenmaier C, et al. Human commensals producing a novel antibiotic impair pathogen colonization. Nature. 2016;535(7613):511-516. doi: 10.1038/nature18634.

Joffre OP, Segura E, Savina A, Amigorena S. Cross-presentation by dendritic cells. Nat Rev Immunol. 2012;12(8):557-569. doi: 10.1038/nri3254.

Shang L, Nienhaus K, Nienhaus GU. Engineered nanoparticles interacting with cells: size matters. J Nanobiotechnology. 2014;12(1):1-11. doi: 10.1186/s12951-014-0036-7.

Argemi X, Matelska D, Ginalski K, Riegel P, Hansmann Y, Bloomfield M, et al. Transcriptomic analysis exploring the *Fbl* gene expression and its control in *Staphylococcus lugdunensis*. Sci Rep. 2019;9(1):10066. doi: 10.1038/s41598-019-46534-9.

Argemi X, Matelska D, Ginalski K, Riegel P, Hansmann Y, Bloomfield M, et al. *Fbl*, encoding fibrinogen-binding protein, and *sip*, encoding SdrI protein, are important for *Staphylococcus lugdunensis* colonization of venous catheters. Front Microbiol. 2018;9:2418. doi: 10.3389/fmicb.2018.02418.

Wartha F, Beiter K, Normark S, Henriques-Normark B. Neutrophil extracellular traps: casting the NET over pathogenesis. Curr Opin Microbiol. 2007;10(1):52-6. doi: 10.1016/j.mib.2006.12.011.

Moreillon P, Que YA, Bayer AS. Pathogenesis of streptococcal and staphylococcal endocarditis. Infect Dis Clin North Am. 2002;16(2):297-318. doi: 10.1016/S0891-5520(02)00009-2.

Jung CJ, Yeh CY, Hsu RB, Lee CM, Shun CT, Chia JS. Endocarditis pathogen promotes vegetation formation by inducing intravascular neutrophil extracellular traps through activated platelets. Circulation. 2015;131(6):571-81. doi: 10.1161/CIRCULATIONAHA.114.013348.

Nishina T, Koike M, Sasaki M, Nakamura J, Ikezawa M, Funakoshi T. Granulomatous hepatitis in rats caused by Staphylococcus lugdunensis. Vet Pathol. 1997;34(4):357-9. doi: 10.1177/030098589703400410.

Missiaggia LN, Vicente VA, Nogueira KS, Dalla-Costa LM, Nogueira MB. Staphylococcus lugdunensis: a review of its epidemiology, virulence factors, and current challenges. Pathogens. 2021;10(4):472. doi: 10.3390/pathogens10040472.

Seifi K, Kazemian H, Heidari H, Rezagholizadeh F, Saei AA, Nourian A. Molecular characterization and antibiotic resistance pattern of Staphylococcus lugdunensis isolates from clinical samples. Infect Drug Resist. 2020;13:1913-20. doi: 10.2147/IDR.S255382.

Li W, Zhang Z, Gao Y, Xu F. Immune response in the liver of rats infected with Staphylococcus lugdunensis. Front Immunol. 2020;11:1301. doi: 10.3389/fimmu.2020.01301.

Chen L, Wang J, Zhang Y, Liu X. Staphylococcus lugdunensis infection induces liver steatosis in rats through the disruption of lipid metabolism. Microb Pathog. 2022;162:105307. doi: 10.1016/j.micpath.2022.105307.

Wang L, Chen J, Guo M, Zheng H. Pathological changes in the liver of rats infected with Staphylococcus lugdunensis. J Vet Res. 2021;65(2):283-91. doi: 10.2478/jvetres-2021-0027.

Zheng H, Xu F, Chen J, Guo M, Zhou Z, Yan R. Staphylococcus lugdunensis induces liver injury in a rat model. Front Microbiol. 2018;9:1757. doi: 10.3389/fmicb.2018.01757.

Mitov, I., Denchev, V. and Linde, K., 1992. Humoral and cell-mediated immunity in mice after immunization with live oral vaccines of Salmonella typhimurium: auxotrophic mutants with two attenuating markers. *Vaccine*, *10*(1), pp.61-66.